Selective Synthesis of a Salt and a Cocrystal of the Ethionamide-Salicylic Acid System

Supporting Information

SELECTIVE SYNTHESIS OF A SALT AND A COCRYSTAL OF THE ETHIONAMIDE-SALICYLIC ACID SYSTEM

Davide Bernasconi, Simone Bordignon, Federica Rossi, Emanuele Priola, Carlo Nervi, Roberto Gobetto, Dario Voinovich, Dritan Hasa, Nghia Tuan Duong, Yusuke Nishiyama, Michele R. Chierotti

Table S1a. Fractional Atomic Coordinates ($\times 10^4$) and Equivalent Isotropic Displacement Parameters ($Å^2 \times 10^3$) for ETH^+SAL^-. U_{eq} is defined as 1/3 of the trace of the orthogonalized U_{IJ} tensor.

Atom	*x*	*y*	*z*	U(eq)
S9A	4752(5)	1332(8)	6104(4)	71.9(8)
O8*	1468.4(16)	-3769(3)	8574.8(14)	72.2(7)
C6	991(2)	1386(4)	5868(2)	54.5(8)
C1*	1656(2)	-3694(4)	7161.4(18)	44.6(7)
N1	1223.2(17)	1400(3)	6722.1(16)	50.5(7)
O10*	173.0(17)	-3073(4)	5963.6(14)	88.0(8)
O9*	143.7(15)	-2874(3)	7501.1(14)	71.1(7)
C2	2177(2)	1058(4)	7240.1(19)	45.8(7)
C3	2939(2)	731(4)	6863.0(18)	48.9(8)
N8	3372.5(18)	-336(4)	4836.3(16)	65.1(8)
C4	2729.4(19)	720(4)	5981.5(19)	44.9(7)
C5	1729(2)	1040(4)	5474(2)	51.4(8)
C10	2332(2)	1158(4)	8190.2(19)	61.9(9)
C7*	1069(2)	-3447(4)	7805(2)	53.3(8)
C7	3596(2)	459(4)	5598.6(19)	53.0(8)
C3*	1735(3)	-3821(4)	5704(2)	69.3(10)
C2*	1177(2)	-3532(4)	6278(2)	54.1(8)
C4*	2760(3)	-4238(4)	5998(3)	72.4(10)
C6*	2696(2)	-4111(4)	7430(2)	59.6(9)
C11	3433(3)	890(6)	8739(2)	87.2(12)
C5*	3252(3)	-4380(5)	6864(2)	69.6(10)
S9B	4763(17)	760(30)	6204(15)	124(8)

Table S2a. Anisotropic Displacement Parameters ($Å^2 \times 10^3$) for ETH^+SAL^-. The Anisotropic displacement factor exponent takes the form: $-2\pi^2[h^2a^{*2}U_{11}+2hka^*b^*U_{12}+\ldots]$.

Atom	U_{11}	U_{22}	U_{33}	U_{23}	U_{13}	U_{12}
S9A	36.1(11)	124.3(17)	57.7(17)	-33.0(14)	17.5(11)	-15.2(10)
O8*	55.2(13)	121(2)	39.7(15)	17.9(13)	13.2(11)	9.3(12)
C6	39.6(17)	75(2)	46(2)	-5.2(16)	8.3(15)	3.3(14)
C1*	44.9(17)	49.2(17)	40.0(19)	6.1(13)	12.9(14)	-3.2(13)
N1	40.9(14)	64.7(16)	50.7(18)	-8.6(13)	20.8(13)	-0.1(11)
O10*	55.5(15)	153(2)	45.8(15)	21.3(16)	0.2(11)	-0.1(15)
O9*	42.4(13)	115.0(18)	59.3(15)	30.6(13)	20.1(11)	8.3(12)
C2	42.7(17)	54.0(18)	42.2(19)	-4.5(13)	14.6(14)	-4.0(14)
C3	39.0(16)	72(2)	34.9(19)	-2.5(14)	9.2(13)	1.3(14)
N8	42.7(14)	111(2)	46.7(18)	-15.5(15)	21.5(13)	-9.8(14)
C4	35.9(16)	57.8(18)	42.2(19)	-5.7(14)	13.5(13)	-2.4(13)
C5	43.4(17)	71(2)	41.1(19)	-2.6(15)	14.9(14)	0.9(15)
C10	66(2)	80(2)	45(2)	-9.8(16)	25.0(17)	-7.0(17)
C7*	40.5(17)	67(2)	52(2)	14.0(16)	13.2(16)	-5.7(15)
C7	41.3(17)	82(2)	36.8(19)	-6.2(16)	12.7(14)	0.5(15)
C3*	87(3)	78(2)	45(2)	0.0(17)	23(2)	-1(2)
C2*	52.2(19)	64(2)	43(2)	7.1(15)	9.2(16)	-3.5(15)
C4*	94(3)	70(2)	69(3)	-3.3(19)	49(2)	9(2)
C6*	52.2(19)	75(2)	51(2)	5.7(16)	14.6(16)	3.7(16)
C11	91(3)	125(3)	39(2)	-3(2)	8(2)	18(2)
C5*	61(2)	88(2)	68(3)	7.2(19)	32(2)	17.9(18)
S9B	51(4)	250(20)	77(6)	-27(10)	23(4)	-16(10)

Table S3a. Bond Lengths for ETH^+SAL^-.

Atom	Atom	Length/Å		Atom	Atom	Length/Å
S9A	C7	1.668(7)		C2	C10	1.502(4)
O8*	C7*	1.234(3)		C3	C4	1.381(4)
C6	N1	1.334(3)		N8	C7	1.318(4)
C6	C5	1.366(4)		C4	C5	1.389(4)
C1*	C7*	1.505(4)		C4	C7	1.500(4)
C1*	C2*	1.400(4)		C10	C11	1.515(4)
C1*	C6*	1.386(4)		C7	S9B	1.62(2)
N1	C2	1.347(3)		C3*	C2*	1.383(4)
O10*	C2*	1.352(3)		C3*	C4*	1.368(5)
O9*	C7*	1.278(3)		C4*	C5*	1.377(5)
C2	C3	1.372(4)		C6*	C5*	1.368(4)

Table S4a. Bond Angles for $ETH^{+}SAL^{-}$.

Atom	Atom	Atom	Angle/°	Atom	Atom	Atom	Angle/°
N1	C6	C5	120.7(3)	O8*	C7*	O9*	123.0(3)
C2*	C1*	C7*	121.7(3)	O9*	C7*	C1*	115.6(3)
C6*	C1*	C7*	120.5(3)	N8	C7	S9A	123.4(3)
C6*	C1*	C2*	117.8(3)	N8	C7	C4	117.0(2)
C6	N1	C2	122.9(2)	N8	C7	S9B	123.1(8)
N1	C2	C3	117.8(3)	C4	C7	S9A	119.4(3)
N1	C2	C10	117.1(2)	C4	C7	S9B	118.7(8)
C3	C2	C10	125.0(3)	C4*	C3*	C2*	120.1(3)
C2	C3	C4	121.0(3)	O10*	C2*	C1*	121.6(3)
C3	C4	C5	119.0(3)	O10*	C2*	C3*	118.3(3)
C3	C4	C7	119.1(2)	C3*	C2*	C1*	120.1(3)
C5	C4	C7	121.8(3)	C3*	C4*	C5*	121.0(3)
C6	C5	C4	118.6(3)	C5*	C6*	C1*	122.2(3)
C2	C10	C11	114.8(3)	C6*	C5*	C4*	118.8(3)
O8*	C7*	C1*	121.4(3)				

Table S1b. Fractional Atomic Coordinates ($\times 10^4$) and Equivalent Isotropic Displacement Parameters ($Å^2 \times 10^3$) for ETH·SAL. U_{eq} is defined as 1/3 of the trace of the orthogonalized U_{IJ} tensor.

Atom	*x*	*y*	*z*	U(eq)
S9	3215.5(6)	473(2)	-36.3(3)	75.1(3)
N1	1227.3(18)	-3107(6)	1514.4(8)	63.9(6)
C2	1122(2)	-4071(7)	1060.2(10)	59.9(7)
C5	2831(2)	-745(7)	1321.3(9)	62.7(8)
C4	2727(2)	-1730(7)	851.0(9)	53.7(7)
C3	1858(2)	-3399(7)	723.9(9)	59.4(7)
C6	2061(2)	-1468(8)	1637.2(10)	69.6(8)
N8	4480.2(19)	-1558(7)	635.8(8)	79.8(8)
C7	3534(2)	-990(7)	490.2(9)	58.6(7)
C10	161(3)	-5934(9)	940.2(13)	86.8(11)
O10*	4785.5(16)	4881(5)	1517.4(7)	73.5(6)
O9*	5176.0(15)	852(6)	2846.9(7)	76.4(7)
O8*	4176.1(16)	3632(6)	2352.8(7)	79.9(6)
C7*	4969(2)	2140(8)	2432.9(10)	61.9(8)
C1*	5760.4(19)	1692(7)	2067.1(8)	52.8(7)
C2*	5625(2)	3070(7)	1619.3(9)	57.5(7)
C4*	7203(2)	860(8)	1362.0(12)	76.0(9)
C6*	6634(2)	-97(7)	2149.4(10)	64.3(8)
C3*	6356(2)	2638(8)	1268.2(10)	70.1(9)
C5*	7354(2)	-502(8)	1801.2(11)	74.5(9)
C11A	-689(7)	-4230(20)	807(4)	83(3)
C11B	-420(12)	-5050(40)	530(5)	221(11)

Table S2b. Anisotropic Displacement Parameters ($Å^2 \times 10^3$) for ETH·SAL. The anisotropic displacement factor exponent takes the form: $-2\pi^2[h^2a^{*2}U_{11}+2hka^*b^*U_{12}+\ldots]$.

Atom	U_{11}	U_{22}	U_{33}	U_{23}	U_{13}	U_{12}
S9	67.1(5)	108.9(7)	50.1(5)	16.6(4)	9.8(4)	10.5(5)
N1	53.7(15)	87.4(17)	51.3(14)	0.7(13)	10.6(11)	1.0(14)
C2	53.7(17)	71.3(19)	54.6(17)	3.1(14)	2.4(13)	1.6(15)
C5	50.4(16)	90(2)	48.3(15)	-3.6(14)	5.6(13)	-5.4(15)
C4	47.6(16)	67.1(17)	46.8(15)	3.2(13)	6.2(12)	6.1(14)
C3	61.3(19)	73.1(18)	44.1(14)	-0.7(14)	5.0(13)	2.6(16)
C6	61.3(19)	103(2)	44.5(15)	-5.8(16)	7.2(14)	-0.4(19)
N8	53.6(16)	133(2)	54.2(14)	24.8(15)	13.0(12)	4.0(16)
C7	51.4(17)	77(2)	47.8(15)	1.7(14)	7.3(13)	4.8(15)
C10	76(2)	99(3)	85(2)	3(2)	5.7(19)	-25(2)
O10*	59.8(13)	102.3(16)	58.6(12)	14.4(11)	3.6(10)	10.2(12)
O9*	59.4(13)	118.9(18)	51.8(12)	8.4(12)	12.2(10)	11.3(12)
O8*	55.3(13)	121.8(18)	63.3(12)	8.1(13)	11.1(10)	19.0(13)
C7*	52.1(18)	82(2)	51.6(17)	-2.3(15)	3.0(14)	-1.6(17)
C1*	43.6(15)	69.5(17)	44.9(14)	-6.3(13)	-0.1(12)	-6.1(14)
C2*	48.9(16)	72.3(18)	51.2(16)	-4.4(14)	1.5(13)	-6.6(15)
C4*	60(2)	103(3)	67(2)	-14.3(19)	21.8(16)	0.1(19)
C6*	58.1(18)	84(2)	50.1(16)	-6.0(14)	-0.3(14)	4.0(16)
C3*	70(2)	91(2)	49.1(16)	-1.0(16)	10.4(15)	-9.0(19)
C5*	57.9(19)	101(3)	64.4(19)	-13.4(18)	5.9(15)	13.5(17)
C11A	51(4)	67(4)	131(8)	15(5)	8(5)	5(4)
C11B	187(16)	320(20)	141(12)	111(13)	-103(10)	-172(15)

Table S3b. Bond Lengths for ETH·SAL.

Atom	Atom	Length/Å		Atom	Atom	Length/Å
S9	C7	1.640(3)		C10	C11B	1.398(13)
N1	C2	1.341(3)		O10*	C2*	1.355(3)
N1	C6	1.320(4)		O9*	C7*	1.303(3)
C2	C3	1.401(4)		O8*	C7*	1.221(3)
C2	C10	1.502(4)		C7*	C1*	1.495(4)
C5	C4	1.386(4)		C1*	C2*	1.392(4)
C5	C6	1.398(4)		C1*	C6*	1.378(4)
C4	C3	1.367(4)		C2*	C3*	1.409(4)
C4	C7	1.520(4)		C4*	C3*	1.351(4)
N8	C7	1.295(3)		C4*	C5*	1.370(4)
C10	C11A	1.359(9)		C6*	C5*	1.390(4)

Table S4b. Bond Angles for ETH·SAL.

Atom	Atom	Atom	Angle/°		Atom	Atom	Atom	Angle/°
C6	N1	C2	117.3(2)		C11B	C10	C2	116.6(6)
N1	C2	C3	122.2(3)		O9*	C7*	C1*	115.9(3)
N1	C2	C10	115.1(3)		O8*	C7*	O9*	121.6(2)
C3	C2	C10	122.7(3)		O8*	C7*	C1*	122.5(3)
C4	C5	C6	119.7(3)		C2*	C1*	C7*	120.2(3)
C5	C4	C7	122.0(2)		C6*	C1*	C7*	122.6(3)
C3	C4	C5	116.8(2)		C6*	C1*	C2*	117.2(2)
C3	C4	C7	121.2(2)		O10*	C2*	C1*	120.1(2)
C4	C3	C2	120.6(2)		O10*	C2*	C3*	119.0(3)
N1	C6	C5	123.4(3)		C1*	C2*	C3*	120.9(3)
C4	C7	S9	121.9(2)		C3*	C4*	C5*	119.8(3)
N8	C7	S9	123.4(2)		C1*	C6*	C5*	121.5(3)
N8	C7	C4	114.7(2)		C4*	C3*	C2*	120.2(3)
C11A	C10	C2	115.0(5)		C4*	C5*	C6*	120.4(3)

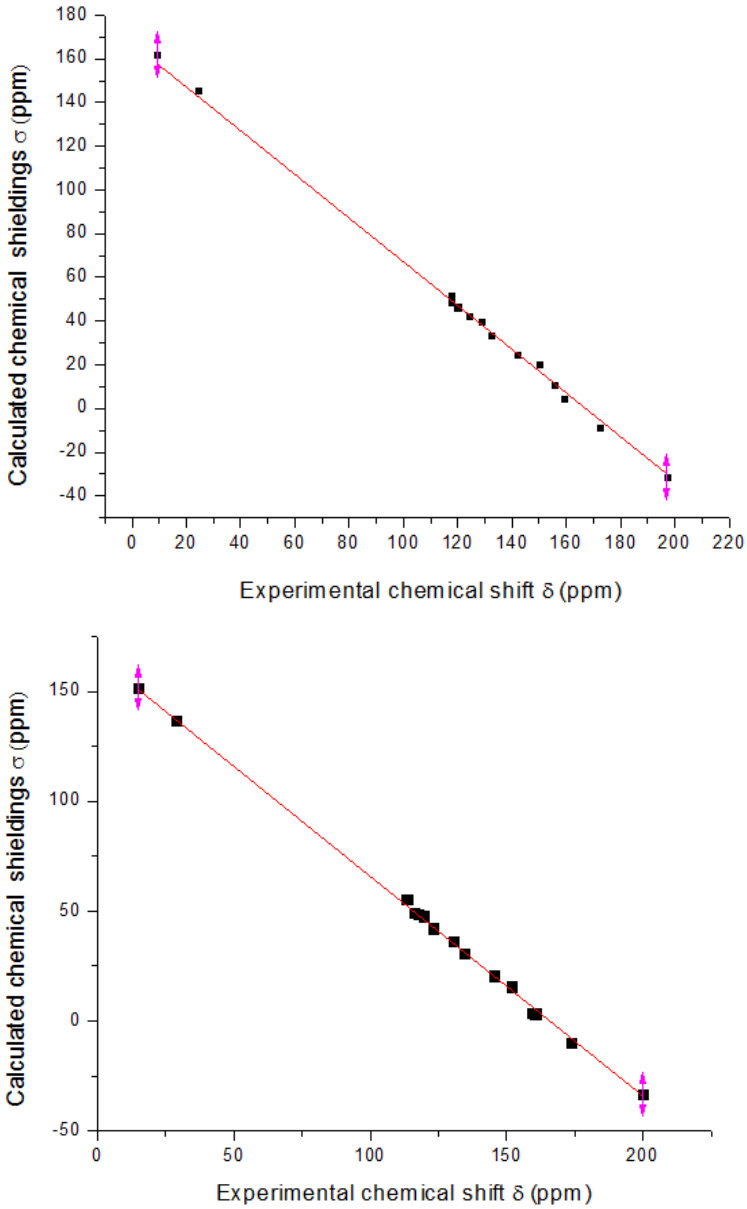

Figure S1. Plots of the experimental ^{13}C chemical shifts $\delta_{(exp)}$ against the GIPAW-calculated ^{13}C chemical shieldings (σ) for the salt (top) and cocrystal (bottom). The linear regression model with slope constrained to −1 was applied to find the best fit to the data. The value of σ_{ref} is determined by the intercepts with the y axis, which are 167.13 and 165.86 ppm for the salt and cocrystal, respectively.

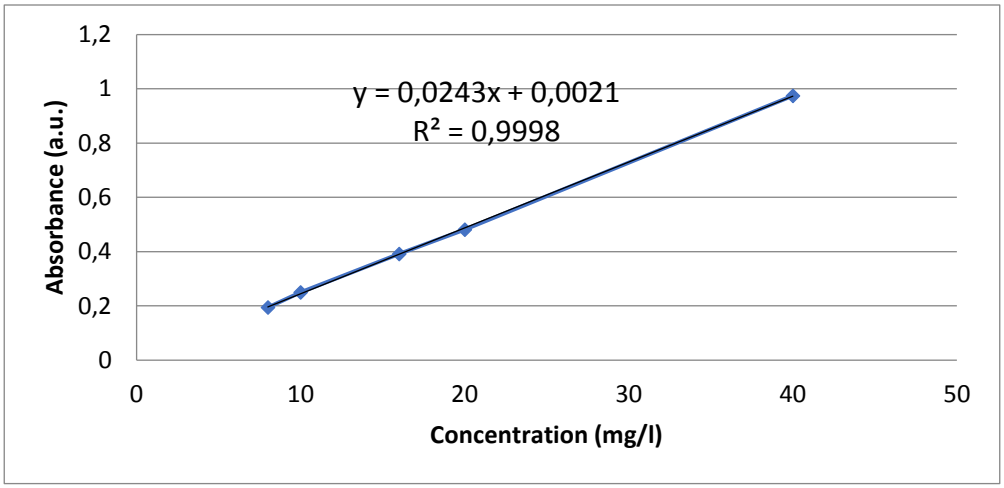

Figure S2. Calibration curve for ETH dissolution were carried out in water (pH 7.4 phosphate buffer) at 37°C.

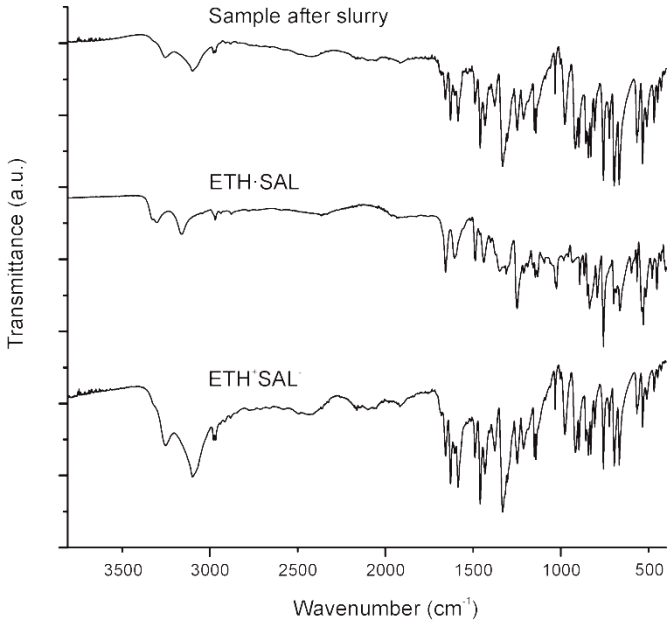

Figure S3. FTIR-ATR spectrum of the competitive slurry sample after 48 hours, compared to ETH·SAL and $ETH^{+}SAL^{-}$ spectra.

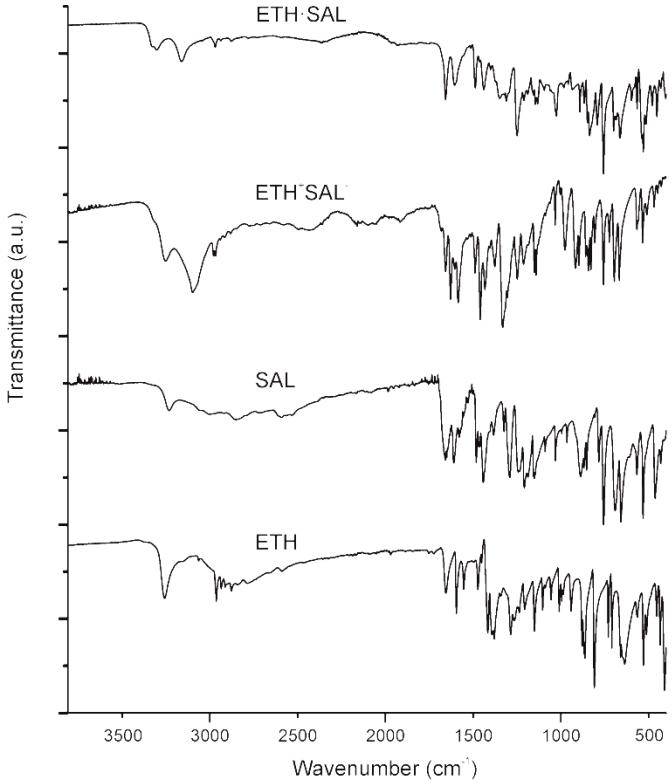

Figure S4. FTIR-ATR spectra of ETH·SAL and $ETH^{+}SAL^{-}$, compared to the starting materials.

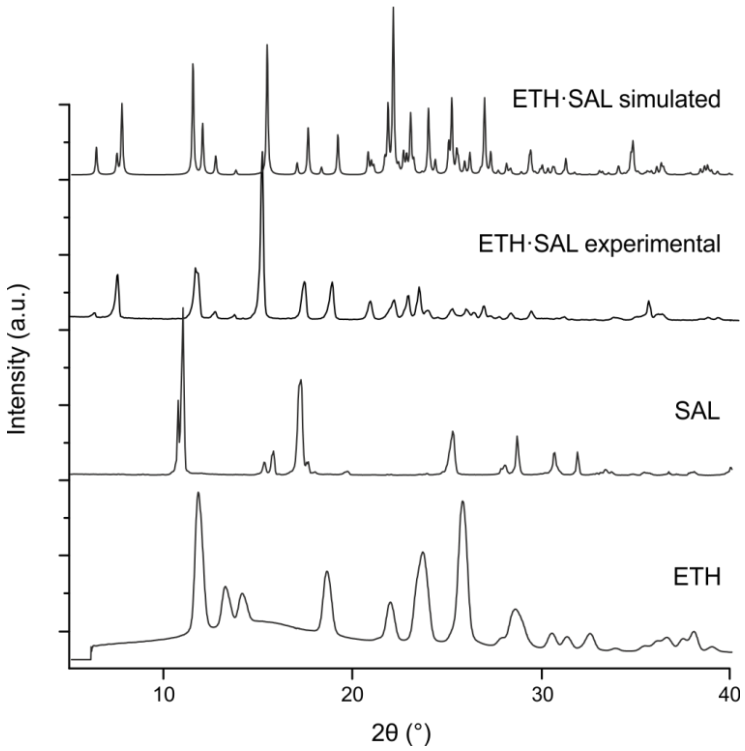

Figure S5. Experimental and simulated PXRD patterns of ETH·SAL, with respect to the starting materials.

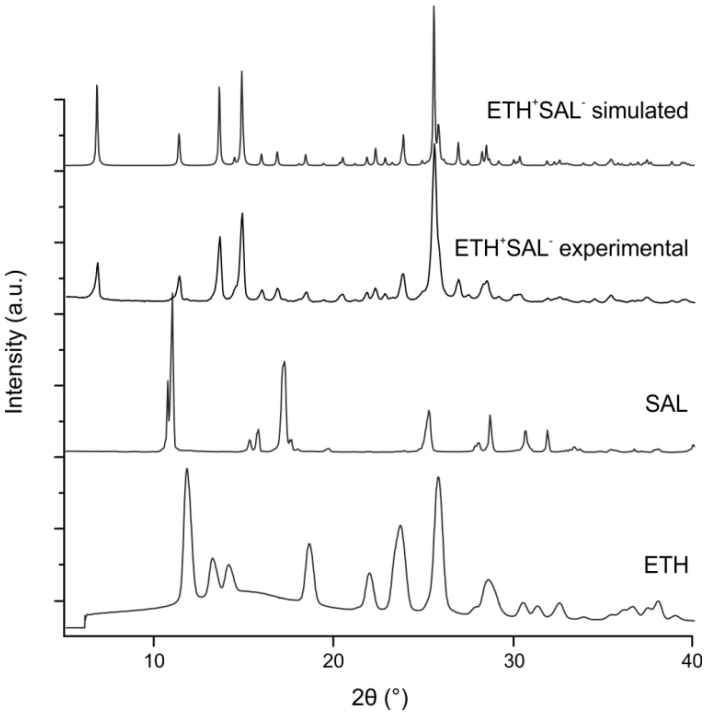

Figure S6 Experimental and simulated PXRD patterns of $ETH^{+}SAL^{-}$, with respect to the starting materials.

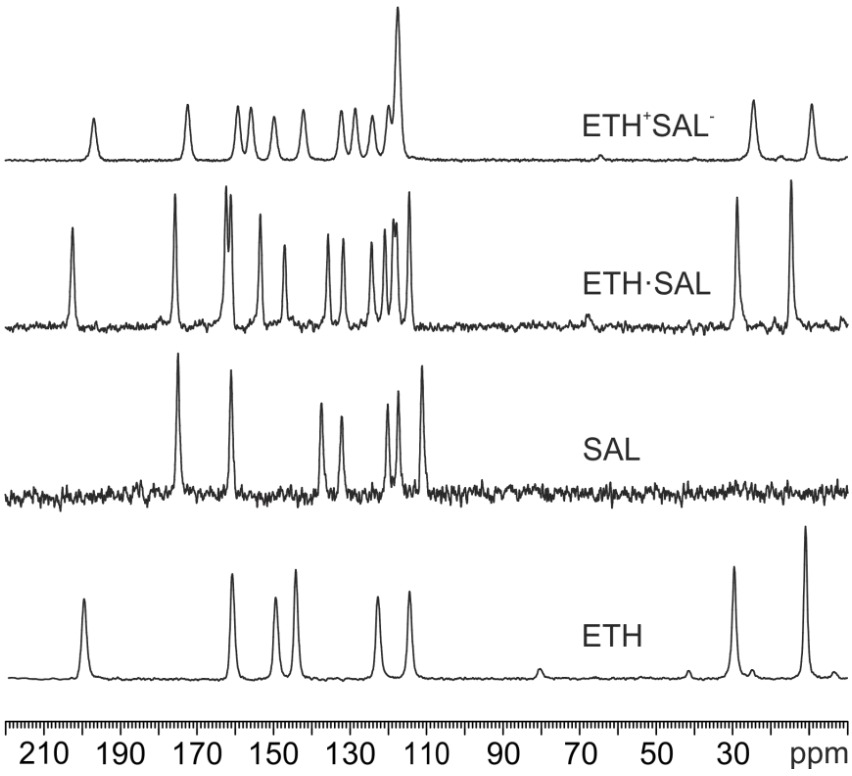

Figure S7. ^{13}C (150.9 MHz) CPMAS spectra of ETH·SAL and $ETH^{+}SAL^{-}$, compared to pure ETH and pure SAL, recorded at 20 kHz at room temperature.

Table S5. ^{13}C, ^{15}N and ^{1}H chemical shift assignments for both polymorphs and starting materials.

Atom	ETH	SAL	$ETH^{+}SAL^{-}$	ETH·SAL
	(ppm)	(ppm)	(ppm)	(ppm)
^{13}C				
2	161.0		155.8	159.4
3	122.9		124.1	123.0
4	149.6		149.9	151.8
5	114.6		117.5	113.5
6	144.4		142.2	145.5
7	199.7		197	200.1
10	29.7		24.4	28.9
11	11.1		9.2	14.9
1*		162.1	117.5	116.2
2*		138.5	159.4	160.6
3*		121.1	119.9	117.5
4*		111.8	132.3	134.4
5*		133.2	119.9	119.6
6*		118.0	128.7	130.4
7*		176.0	172.4	173.8
^{15}N				
8	154.0		147.4	148.7
1	309.0		211.9	273.4
^{1}H				
8			10.8	10.3/8.7
9*			18.4	17.3
3/5/6/3*/4*/5*/6*			7.1/6.7	5.8/6.6/7.9
10/11			1.2/2.4	1.08
10*			12.6	11.6

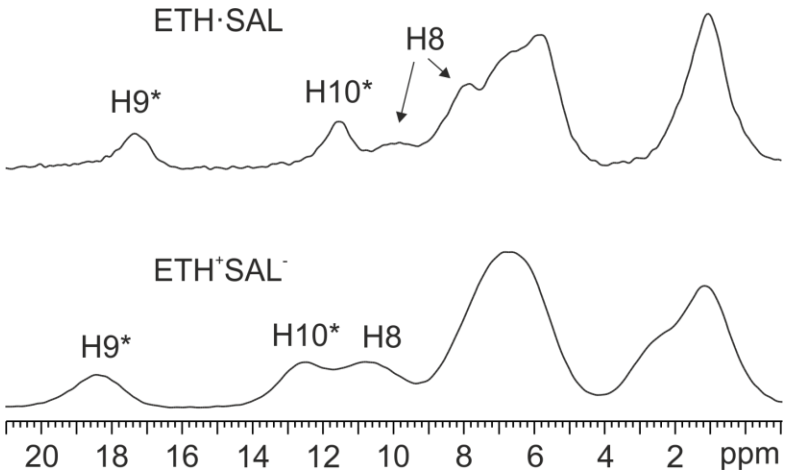

Figure S8. ^{1}H (600.1 MHz) MAS spectra of ETH·SAL and $ETH^{+}SAL^{-}$, recorded at 70 kHz at room temperature.

Analysis of the 2D ^{1}H-{^{14}N} *D*-HMQC spectra

Figure 4 shows the 2D ^{1}H-{^{14}N} *D*-HMQC spectra of ETH^{+}SAL^{-} and ETH·SAL, respectively, in which the N-H correlations for N1 and N8 atoms of ETH are observed. These spectra allow the ^{1}H assignment of the thioamidic N-H (H8) and pyridinic N^{+}-H or N···H (H9*) resonances as follows: at 10.8 (H8) and 18.4 (H9*) ppm for ETH^{+}SAL^{-} and at 10.3/8.7 (H8) and 17.3 (H9*) ppm for ETH·SAL. Concerning ^{14}N, it suffers from a strong quadrupolar interaction, stemming from the interaction between an intrinsic quadrupolar moment (because of spin-1 nucleus) and the electric field gradient (because of the surrounding environment). While the ^{14}N line shape is dominated by the first-order quadrupolar broadening at the static conditions, MAS gets rid of the broadening and results in a set of spikelet spinning sidebands. These sidebands are folded in the indirect (^{14}N) dimension of *D*-HMQC spectra, giving a sharp peak at the isotropic peak positions. In the end, the ^{14}N resonance positions depend on both the isotropic chemical shift (σ_{iso}) and an additional second-order isotropic quadrupolar shift. Since the quadrupolar coupling strongly depends on the surrounding environment of the quadrupolar nucleus, the additional shift is more significant for asymmetric nitrogen sites and *vice versa*. This perfectly agrees with the experimental ^{14}N shifts found in the 2D ^{1}H-{^{14}N} *D*-HMQC spectra of ETH^{+}SAL^{-} and ETH·SAL, confirming the ionic/neutral character of the samples:

- in the case of ETH^{+}SAL^{-}, the ^{14}N shifts of N1 and N8 slightly differ from each other implying that the environments surrounding the two nitrogen sites are similar in terms of symmetry and thereby suggesting a protonation of N1 (NH^{+} group);
- the ^{14}N shift of N1 in ETH·SAL is much larger than that of N8 (nearly 400 ppm), indicating a less symmetric surrounding environment which agrees with a farther hydrogen position from the nitrogen (N···H-O).

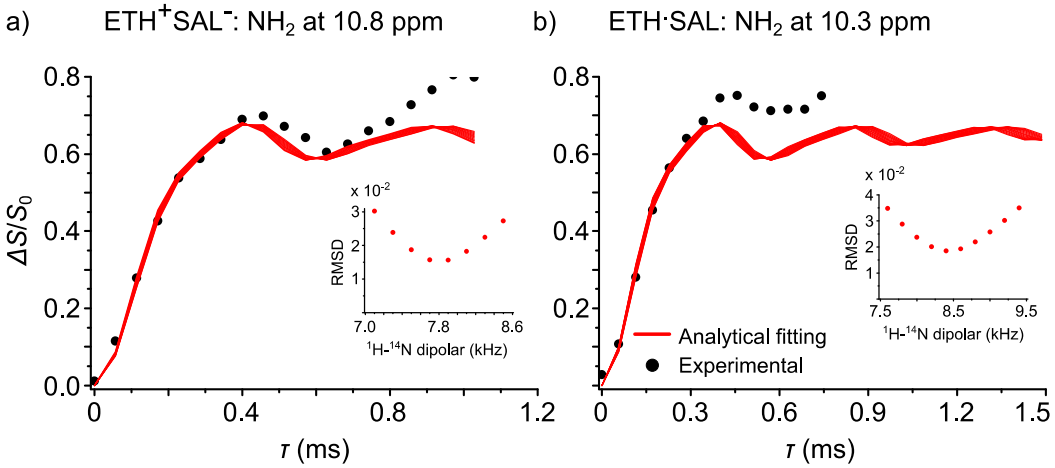

Figure S9. Experimental ^{14}N-^{1}H fraction curves (dots) achieved by PM-S-RESPDOR of (a) ETH^{+}SAL^{-} and (b) ETH·SAL at ^{1}H chemical shifts of 10.8 and 10.3 ppm, respectively and analytical fitting curves (solid red lines). The fitting was up to 0.40 ms for ETH^{+}SAL^{-} and 0.34 ms for ETH·SAL. The insets show the best fitting ^{1}H-^{14}N dipolar coupling based on root mean square deviation analysis. The experimental $\Delta S/S_0$ data larger than 0.8 are not shown in the figures. The obtained values of N-H distance for these NH$_2$ sites are 1.04 and 1.01 Å for ETH^{+}SAL^{-} and ETH·SAL, respectively.

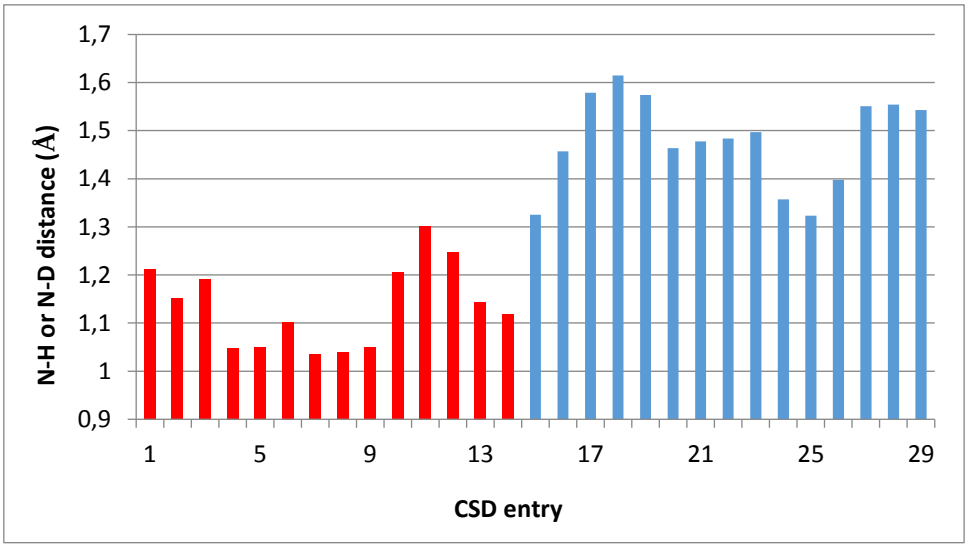

Figure S10. N-H or N-D distances of the 29 CSD structures, obtained by neutron diffraction, containing pyridine-carboxylic acid interaction (14 salt structures are indicated in red, while 15 cocrystal structures are indicated in blue).

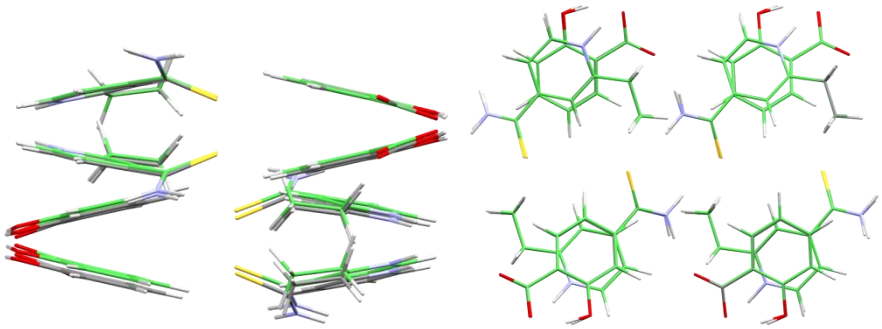

Figure S11. Superposition of experimental and DFT-optimized (green) $ETH^{+}SAL^{-}$ structures.

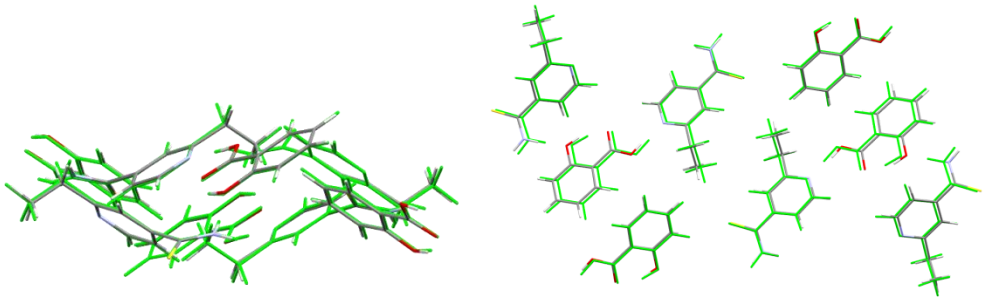

Figure S12. Superposition of experimental and DFT-optimized (green) ETH·SAL structures.

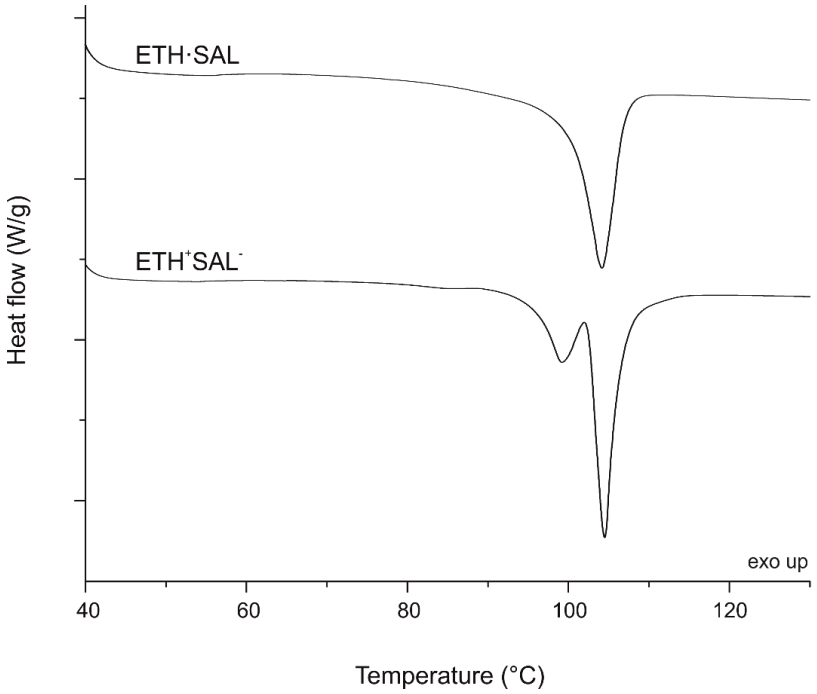

Figure S13. DSC curves of $ETH^{+}SAL^{-}$ and ETH·SAL.

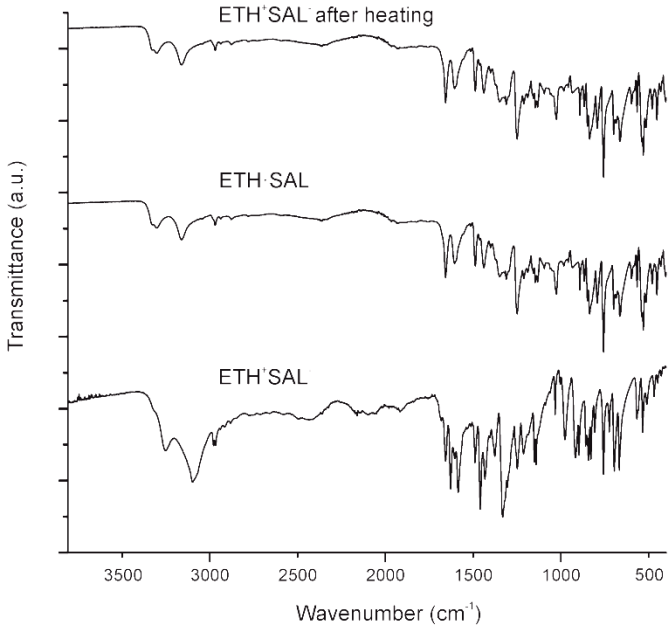

Figure S14. FTIR-ATR spectrum of $ETH^{+}SAL^{-}$ sample after heating to 100 °C, compared to the spectra of ETH·SAL and $ETH^{+}SAL^{-}$.

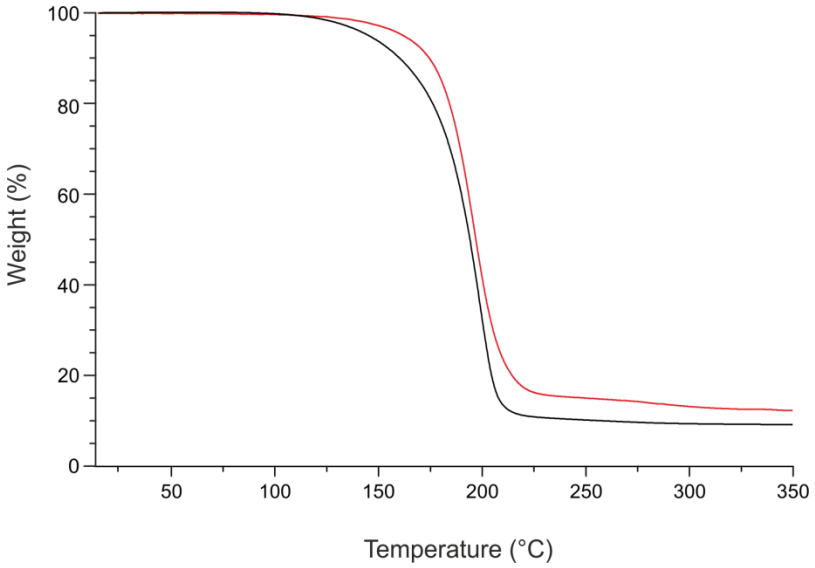

Figure S15. TGA curves of $ETH^{+}SAL^{-}$ (black) and ETH·SAL (red).